Research

Iron-doped catalyst synthesis in heterogeneous Fenton like process for dye degradation and removal: optimization using response surface methodology

Abderrazzak Adachi[1] · Faiçal El Ouadrhiri[1] · Ebraheem Abdu Musad Saleh[2] · Raed H. Althomali[2] · Asmaa F. Kassem[2,3] · El Manssouri Ibtissam[2] · Moharam Marwa Mostafa[2] · Kakul Husain[2] · Noureddine Eloutassi[1] · Amal Lahkimi[1]

Abstract

Iron-doped hydrochar can effectively remove the methyl orange dye (MO). In this study, iron-doped hydrochar (5% Fe@ BC) was successfully synthesized through a two-step hydrothermal carbonization (HTC) process, using $FeSO_4.7H_2O$ and sawdust. It was subsequently employed for MO removal. The characterization of the synthesized Fenton-like catalyst (5% Fe@BC) was conducted, using scanning electron microscopy, Fourier-transform infrared and X-ray diffraction techniques to confirm the presence of iron species. The effects of different operating parameters such as catalyst mass, H_2O_2 concentration, solution pH, organic pollutant concentration, and reaction temperature have been examined. The Box-Behnken design combined with three factors: catalyst mass X_1, temperature X_2, organic pollutant concentration X_3. The response surface methodology coupled with Box-Behnken Design was used to optimize the key variables and response. With this approach, an exhaustive assessment of the variables influencing the optimization process was performed. A significant quadratic model was generated through analysis of variance with a P-*value* of 0.0001 and an R^2 of 0.99. This confirms a strong relationship between the variables and the response, as well as a high level of model predictability. The optimum conditions were achieved with a catalyst mass of 0.5 g/L, a temperature of 35.5 °C, and an MO concentration of 50 mg/L. The result indicates that 93% of the discoloration efficiency was achieved within 60 min under the optimal conditions. Iron doping in the (5% Fe@BC) plays a crucial role in the degradation and removal of MO. Therefore, the 5% Fe@BC prepared from sawdust and iron salts ($FeSO_4·7H_2O$) through a two-step HTC process is an inexpensive and effective catalyst for removing organic pollutant from aqueous solutions, using heterogeneous Fenton-like process.

✉ Abderrazzak Adachi, abderrazzak.adachi@usmba.ac.ma; ✉ Faiçal El Ouadrhiri, Faical.elouadrhiri@usmba.ac.ma; Amal Lahkimi, Amal.lahkimi@gmail.com | [1]Laboratory of Engineering, Faculty of Sciences Dhar El Mahraz, Electrochemistry, Modelling and Environment, Sidi Mohamed Ben Abdelah University, Fez, Morocco. [2]Chemistry Department, College of Arts & Science, Prince Sattam Bin Abdulaziz University, Wadi Al-Dawaser, Alkharj, Saudi Arabia. [3]Department of Chemistry of Natural and Microbial Products, National Research Centre, Cairo 12622, Egypt.

Article Highlights

- Novel iron-doped hydrochar (5%Fe@BC) was synthesized by two-step HTC method.
- 5%Fe@BC demonstrated excellent performance in degrading and removing MO.
- Characterized catalyst using SEM, FTIR, and XRD, confirming iron species presence.

- Explored effects of catalyst mass, H_2O_2 concentration, pH, MO concentration, and temperature.
- Employed BBD and RSM for optimization, yielding a significant quadratic model (P = 0.0001, R^2 = 0.99).
- MO removal efficiency achieved 93% under optimal conditions.

1 Introduction

For many years, the treatment of industrial wastewater has been a recurrent problem with significant environmental implications. Among these, the degradation and elimination of dyes produced by the textile industry use a lot of water and toxic chemicals [1]. Most colorants are highly stable, nonbiodegradable. They have toxic, teratogenic, and carcinogenic properties [2]. Methyl orange is extensively utilized in the textile, cosmetics, and paint industries as a predominant colorant. However, it has an anionic characteristic and belongs to the azo group (N=N), making it potentially hazardous to the aquatic environment due to its toxicity [3].

Various methods have been used to remove dyes from wastewater, including Electro Fenton [4, 5], biological methods [6], adsorption [7, 8], coagulation-flocculation [9], and advanced oxidation process [10]. However, these methods have various drawbacks, such as high costs and energy consumption, advanced materials technologies, sludge production. Among the previously mentioned wastewater treatment methods, there is the heterogeneous Fenton-like, which relies on the in-situ generation of hydroxyl radicals (OH·) via Eqs. 1 and 2. This process is increasingly attracting interest in the field of wastewater treatment [11, 12]. The heterogeneous Fenton-like process hinges on the utilization of solid catalysts that are both cost-effective and eco-friendly [13]. Although significant progress has been made in the development of solid catalysts, their application in heterogeneous Fenton-like processes still represents a major challenge.

$$Fe^{2+} + H^+ + H_2O_2 \rightarrow Fe^{3+} + H_2O + HO, \tag{1}$$

$$Fe^{3+} + H_2O_2 \rightarrow Fe^{2+} + H^+ + HOO \tag{2}$$
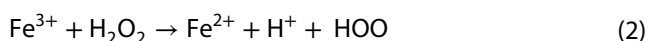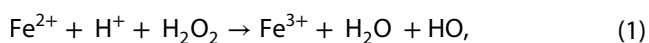
Recently, extensive studies have been carried out for the synthesis of solid catalysts such as nanoscale zerovalent iron [14], ferro ferric oxide nanoparticles [15], cobalt ferrite [16], as well as copper ferrite [17], with a view to their application in the heterogeneous Fenton-like process. However, solid catalysts based on cobalt (Co), copper (Cu) inevitably leach heavy metals, posing a risk to human health and the environment. Iron-based catalysts are attracting increasing demand due to their high surface area and their activity with H_2O_2. In this study, iron salts ($FeSO_4$, $7H_2O$) were used to synthesize an Iron-doped catalyst, utilizing the hydrothermal carbonization procedure. This approach has various advantages over transition metals due to its affordability, non-toxicity, eco-friendliness. The application of sawdust as a heterogeneous Fenton-like catalyst has scarcely been tested for the removal of organic dyes. Recently, the biomaterial-based heterogeneous Fenton process has appeared as a suitable solution to overcome the drawbacks of homogeneous Fenton processes [18]. Currently, the conversion of hydrochar into a high-value catalyst is being increasingly studied and implemented in the field of environmental catalysis [19]. Sawdust, a co-product of the furniture and timber industries, is an abundant and cost-effective source of lignocellulosic material. It is considered as one of the most available rich carbon resources [20]. The carbonization of sawdust has the potential to eliminate organic Micropollutants through the adsorption process [21]. Although the production of activated carbon via pyrolysis is a common method for organic pollutant removal. It has drawbacks such as the need for an inert nitrogen-based environment, high temperatures, high energy consumption, and the requirement for sophisticated equipment [22, 23]. In contrast to pyrolysis, hydrothermal carbonization does not necessitate an inert environment and can be carried out at lower temperatures (ranging from 180 to 350 °C).The hydrochar produced via HTC has been used for wastewater treatment characterized by its porous structure, oxygenated functional groups and aromatic surfaces [24].

Our search is among available ones that revealed a lack of articles, concerning the use of hydrochar prepared from

sawdust for MO dye removal by the heterogeneous Fenton-like process. As a result, the primary objective of our study was the preparation of iron-doped hydrochar from sawdust, using the hydrothermal carbonization method and its utilization for the removal of MO dyes from aqueous solutions. Based on this objective, the sub-objectives of the present study were as follows:

(a) To produce iron-doped hydrochar as a catalyst with Fenton-like properties
(b) To investigate the impact of various parameters in the heterogeneous Fenton process, such as the dosage of the heterogeneous Fenton catalyst, H_2O_2 concentration, solution pH, concentration of the organic pollutant MO, and solution temperature.
(c) To describe the physicochemical characteristics of the produced catalysts
(d) To optimize the decolorization rate using a response surface methodology (RSM) based on the Box-Behnken design (BBD).

This research marks a significant advancement in the development of a biomass-based catalyst for the sustainable degradation and elimination of toxic dyes through the heterogeneous Fenton- like process.
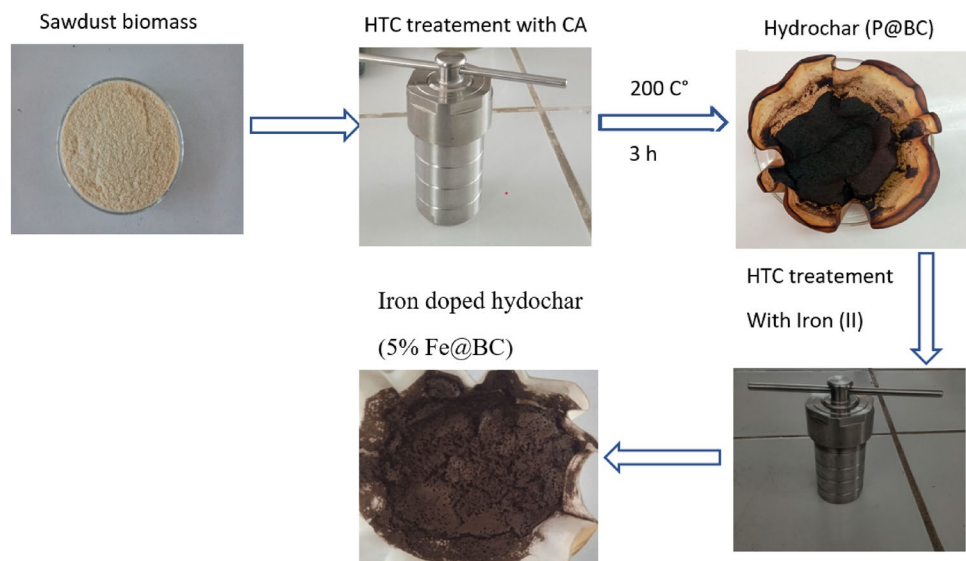
1.1 Material and method

2 Materials

In the Bensouda-Fes region of Morocco, a single type of sawdust sample was collected from a local wood processing facility. The chemicals, including hydrogen peroxide (H_2O_2, 30% by weight), ferrous sulfate heptahydrate ($FeSO_4, 7H_2O$), citric acid ($C_6H_8O_7$), benzoic acid ($C_7H_6O_2$), sodium hydroxide (NaOH $\geq$ 99.99%), sulfuric acid (H_2SO_4, analytical grade $\geq$ 85%), and methyl orange ($C_{14}H_{14}N_3NaO_3S$), were of ACS reagent grade and purchased from Sigma-Aldrich, St. Louis, Missouri, United States (Fig. S1). In the studies, ultrapure water with a resistivity of 18.2 Ω.cm was created using a Millipore Milli-Q water purification system.

2.1 Preparation of the iron-doped catalyst

The sawdust hydrothermal carbonization experiment was realized in a 100 ml autoclave lined with polypropylene, as shown in Fig. 1. In each preparation, 5 g of sawdust were immersed in 50 ml of distilled water to obtain a 1:10 ratio, with manual agitation for 10 min. To enhance the performance of the hydrochar, a 10 mg quantity of citric acid (CA) as an acid catalyst was added to the autoclave before being inserted into the reactor and carefully shut [24, 25]. After this, the autoclave was moved to an oven, where it was warmed to 200 °C for three hours [26]. All experiments were conducted using a consistent heating rate of 5 °C per minute. After this, the autoclave was left to cool down naturally, and the solid residue, known as hydrochar, was obtained through vacuum filtration. Finally, the hydrochar was rinsed with distilled water until it reached a neutral pH and dried overnight in an oven at 105 °C before being stored [27].The hydrochar was named P@BC. The iron-doped hydrochar was prepared using a two-step low-temperature hydrothermal carbonization method. In 50 ml of ionized water, 1 g (5%) of $FeSO_4$, $7H_2O$ was dissolved, (Results for 1% and 3% are not included). Then, 4 g of pristine hydrochar (P@BC) was added to the solution

Fig. 1 Graphical diagram of the preparation of iron-doped hydrochar

Sawdust biomass

HTC treatement with CA

Hydrochar (P@BC)

200 C°

3 h

HTC treatement

With Iron (II)

Iron doped hydochar

(5% Fe@BC)

and stirred slowly for 60 min. The properly mixed solution was then put into an autoclave and given a three-hour hydrothermal treatment at a temperature of 200 °C [28]. The resultant dark precipitates were then filtered, cleaned with ionized water, overnight dried at 80 °C, and placed in a recipient for later use. The hydrochar with iron doping is named 5%Fe@BC.

2.2 Characterization

To examine the sample morphologies, the field emission scanning electron microscope (Hitachi S4800) was employed along with energy dispersive X-ray spectroscopy. This combination allowed for detailed analysis of the sample surfaces and the elemental composition using X-ray spectroscopy. Inductively coupled plasma atomic emission spectroscopy (ICP-AES) was utilized to perform elemental analysis and quantify the concentration of iron in the liquid phase following HTC. This technique allowed for precise measurement of iron content in the analyzed samples. XRD patterns were acquired using a powder X-diffractometer (Expert-pro). Cu K radiation, an acceleration voltage of 40 kV, a 2θ range beginning at 0.02°, and a scanning speed of 6° per minute were all used in the operation of the XRD apparatus. This setup allowed for the characterization and analysis of the crystalline structures present in the samples. Using an FTIR Nicole 5700 model (USA) Fourier-transform infrared spectrophotometer, the surface functional groups of the materials were assessed. The samples were analyzed at a resolution of $4 cm^{-1}$ using KBr pellets.

2.3 Experimental procedure

Experimental batch trials were conducted in a 250 ml glass beaker placed on a magnetic stirrer hotplate (Stuart, SB 162) with a stirring speed of 150 rpm for minutes [29]. For all experiments, a working volume of 100 ml of MO solution at a specific concentration prepared by dilution of the stock solution was used. The MO solution was treated by adding a predetermined quantity of catalyst doped with iron and H_2O_2. Various parameters were changed to evaluate the efficiency of the Fenton-like process in degrading and decolorizing the organic contaminant. The parameters investigated in the study encompassed the catalyst mass, ranging from 0

to 1 g/L, H_2O_2 concentration, ranging from 0 to 10 mM, the solution pH adjusted between 3 and 10, MO concentration, between 20 and 50 mg/L, and the solution temperature, varying from 15 to 50 °C. These parameters were systematically varied to assess their impact on the process performance. During the experimental tests, each parameter was evaluated individually to identify its optimal value, with all other parameters held constant. At specific time points, a sample containing the pollutants was extracted, and subsequently isolated through the process of filtration. This allowed for the concentration of the pollutants in the sample to be assessed and analyzed. The concentration of the pollutants was determined using a UV–visible spectrophotometer (model: 2005, HJD501) at a wavelength of 464 nm, as depicted in Figure S1 [30]. The color removal efficiency was evaluated using Eq. 3 [31]:

$$\text{Discoloration rate (R\%)} = \left(\frac{C_0 - C_t}{C_0} \right) \times 100 \qquad (3)$$

where R (%) is the efficiency of organic matter removal, C_0 (mg/l) and C_t (mg/l) are the initial and final concentration of organic matter, respectively.

2.4 Experimental plan

The BBD model was used to optimize experimental parameters for enhanced degradation and removal of organic contaminants via a Fenton-like process [31, 32]. This statistical approach involved utilizing expert design software to generate a series of batch experiments aimed at achieving optimal results [33]. Three factors with three levels each were used: (i) pollutant dosage (X_1: 20 mg/l, 45 mg/l, 70 mg/l), (ii) catalyst mass (X_2: 0.1 mg/l, 0.55 mg/l, 1 g/l) and (iii) temperature (X_3: 25 °C, 40 °C, 55 °C) these factors were utilized to determine the coefficients of the quadratic model (Table 1). The predicted response, Y_i represents the variables of discoloration rate (R%) calculated by the equation:

$$Y_i = \beta_0 + \sum_{i=1}^{n} (\beta_i X_i) + \sum_{i=1}^{n} (\beta_{ii} X_i^2) + \sum_{i=1}^{n-1} \sum_{j=1}^{n} (\beta_{ij} X_i X_j) + \mathcal{E} \qquad (4)$$

The model consists of various coefficients: β_0 represents the intercept coefficient, β_i represents the linear coefficients, β_{ii} represents the squared coefficients, and β_{ij}

Table 1 Variables and their limits for the box Behnken design of organic matter (MO) degradation

Coded factor	Name	Unit	Minimum	Maximum	Coded Low	Coded High
A: X_1	[MO]	mg/L	20.00	70.00	−1 ↔ 20.00	+1 ↔ 70.00
B: X_2	Catalyst mass	g	0.10	1.00	−1 ↔ 0.10	+1 ↔ 1.00
C: X_3	Temperature	°C	25.00	55.00	−1 ↔ 25.00	+1 ↔ 55.00

represents the interaction coefficients. The variables X_i and Y_j are the coded independent variables, while ε represents the random error [24, 31]. The number of experiments was determined according to the following equation: $2k(k-1) + N_0$ with $N_0 = 4$ central experimental points.

3   Results and discussion

3.1   SEM characterization

Figure 2 presents the comparison of surface morphology between raw sawdust (a), virgin hydrochar prepared by hydrothermal carbonization (b), and 5%Fe@BC-doped catalyst (c). SEM image of raw sawdust in 2a provide information regarding the structure and morphological characteristics. It shown an asymmetrical and highly non-porous surface. In contrast, the structure observed in the SEM image of hydrochar (P@BC) Fig. 2b indicates a layered structure and a well- developed heterogeneous porous surface. Perhaps the porous structure of the hydrochar is created during hydrothermal carbonization [23]. SEM

image of the catalyst 2c shows a highly pronounced morphology of the stacked layer and wrinkled sheet, which could be attributed to the formation of defect-rich structures caused by the incorporation of iron atoms in the virgin hydrochar [34]. Energy-dispersive X-ray spectroscopy (EDS) analysis was conducted to examine the chemical composition of the synthesized heterogeneous catalyst.

Table 2   chemical composition of 5%Fe@BC heterogeneous catalyst

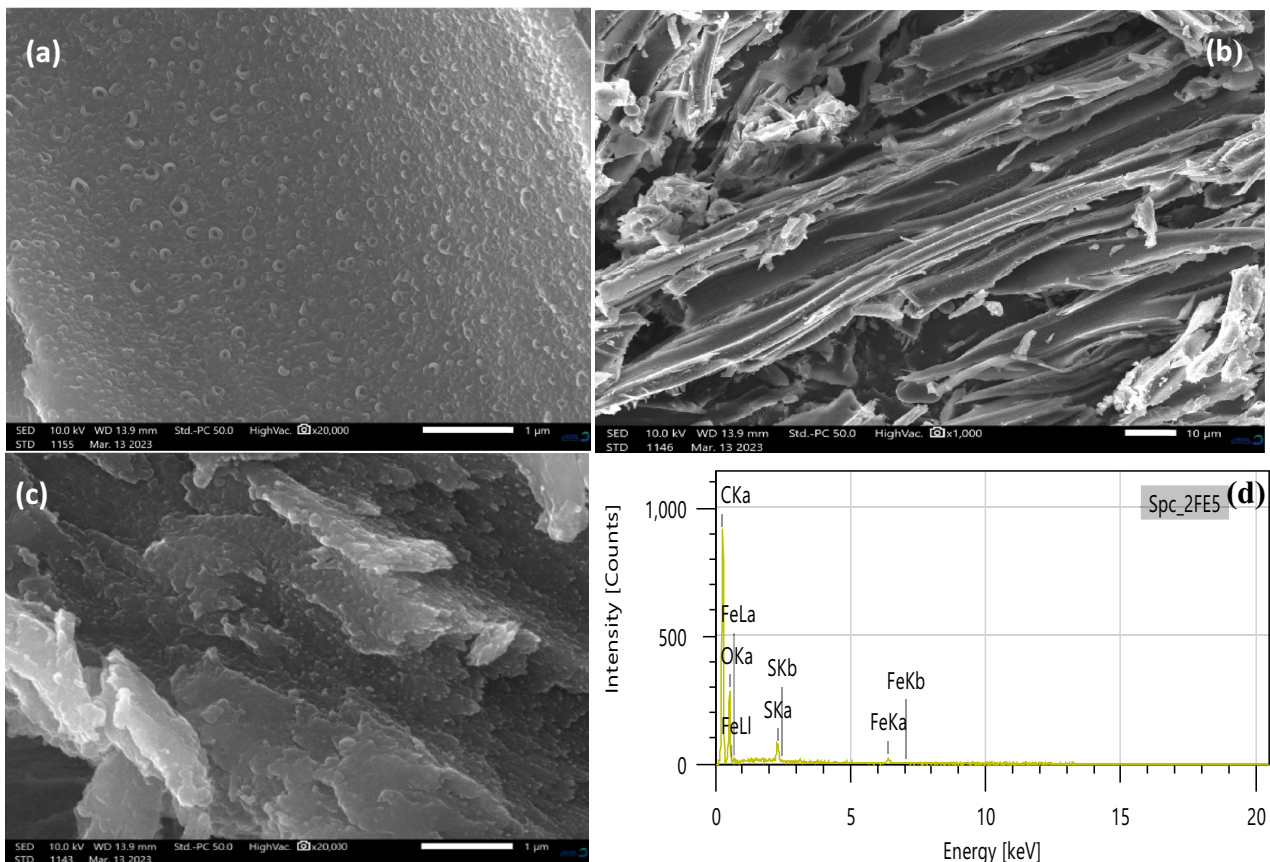| Element	Line	Mass%	Atom%
C	K	63.13 ± 0.35	72.20 ± 0.40
O	K	29.87 ± 0.61	25.65 ± 0.53
S	K	2.38 ± 0.11	1.02 ± 0.05
Fe	K	4.62 ± 0.33	1.14 ± 0.08
Total		100.00	100.00
C	K	63.13 ± 0.35	72.20 ± 0.40
O	K	29.87 ± 0.61	25.65 ± 0.53
S	K	2.38 ± 0.11	1.02 ± 0.05
Fe	K	4.62 ± 0.33	1.14 ± 0.08
Total		100.00	100.00

Fig. 2   Raw sawdust (**a**), virgin hydrochar (**b**), iron-doped hydrochar (**c**), and EDS spectrum (**d**) pictures from scanning electron microscopy (SEM)
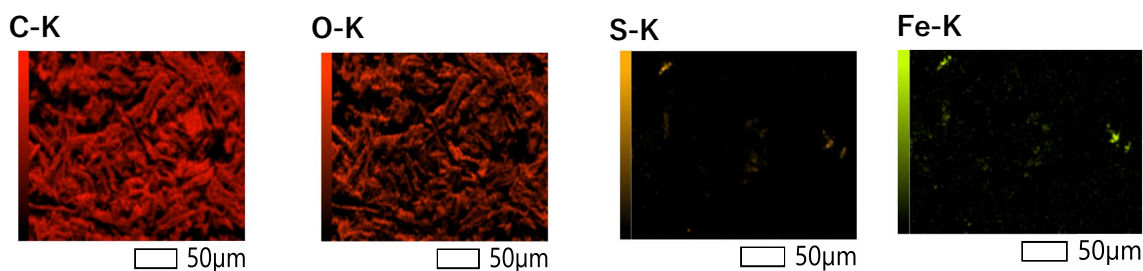
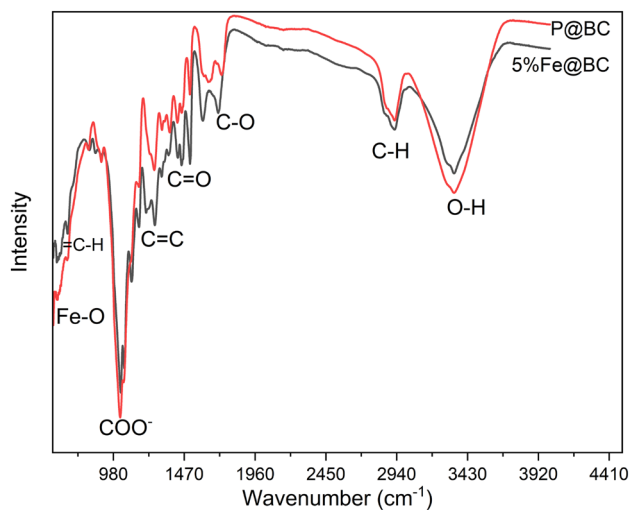**Fig. 3** EDS elements distribution mapping of 5%Fe@BC

Fig. 4 Infrared spectrum of virgin hydrochar P@BC, iron-doped hydrochar 5%Fe@BC

Fig. 5 XRD pattern of pristine hydrochar (P@BC), the iron-doped hydrochar (5%Fe@BC)

The results of this analysis, presented in Table 2 and Fig. 3, show a significant presence of carbon atoms (C), oxygen (O), as well as the presence of iron atoms (Fe) accompanied by certain impurities such as sulfur (S) in small quantities. It is likely that the presence of sulfur (S) and iron (Fe) is attributed to $FeSO_4,7H_2O$, an inorganic compound commonly encountered in the composition of synthesized catalysts. The results indicate that the catalyst effectively incorporates iron elements, demonstrating successful doping.

3.2 FTIR characterization

Figure 4 displays the FTIR spectra of P@BC and 5%Fe@BC. Both spectra exhibit several characteristic peaks that are shared between them. The presence of absorbance peaks within the range of 3200 to 3600 cm^{-1} suggests vibrations associated with the O–H bond. The peaks observed around 2940 cm^{-1} can be attributed to the vibrations of the C–H bonds within the aliphatic group of cellulose. The asymmetric and symmetric stretching modes of the C–H bonds are represented by these vibrations. [35]. The typical
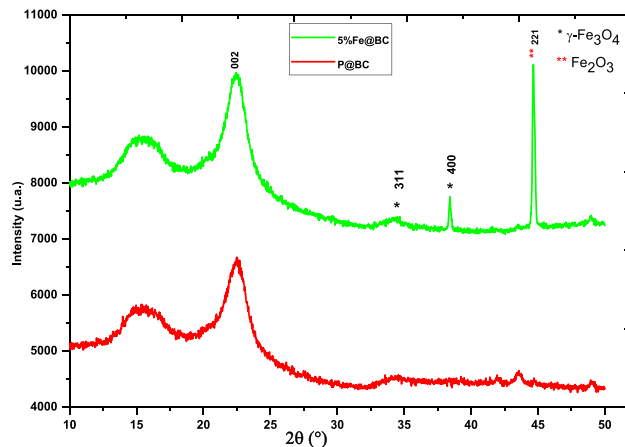
band of aromatic C=C stretching corresponds to the peak at 1360 cm^{-1}. The vibration of the C-O bond results in an absorbance peak at 1702 cm^{-1}, which serves as an indication of the existence of carboxylic acids, ketones [36]. The presence of C–O stretching can be inferred from the absorption band observed around 1835 cm^{-1} [37]. While the peak at 842 cm^{-1} represents the stretching of COO^- bonds, the peak at 1384 cm^{-1} represents =C–H bonding. It is possible to link the 580 cm^{-1} peak in the 5%Fe@BC catalyst to the Fe–O stretching vibration. This finding implies that iron was successfully doped into hydrochar [38].

3.3 XRD analysis

The XRD spectrum shown in Fig. 5 of both P@BC and 5%Fe@BC reveals a broad peak around 22.6°, which corresponds to the (002) plane. This peak indicates the presence of amorphous carbon without crystalline characteristics, suggesting the formation of such carbon during the reduction process [39, 40]. The presence of graphitic carbon can be attributed to the enhancement of hydrothermal carbonization by Fe iron particles. A distinctive

peak emerges at 35.2°, which corresponds to the characteristic (311) plane of γ-Fe$_3$O$_4$ (JCPDS no. 03-065-0390). This peak indicates the formation of γ-Fe$_3$O$_4$ resulting from the reduction of ferric oxide during the hydrothermal carbonization process [41, 42]. An intense peak is observed at 44°, corresponding to the (221) plane of Fe$_2$O$_3$ (JCPDS no. 25-1402) [43]. XRD analysis provides evidence for the existence of graphitic carbon, Fe$_2$O$_3$, and γ-Fe$_3$O$_4$ following the introduction of iron doping.

4 Effects of operating parameters

4.1 Effect of catalyst dosage

Solid catalysts play a crucial role in activating hydrogen peroxide (H$_2$O$_2$) to produce highly potent radicals with the Fenton system [44]. The catalyst dosage is an essential variable in the heterogeneous Fenton approach, it is necessary to establish the applicable dosage. According to Fig. 6, the degradation of MO increases noticeably when the dosage of 5%Fe@BC is increased from 0 to 1g/l. Previous studies have shown similar outcomes, with increased H$_2$O$_2$ activity when the catalyst dose is increased [45, 46]. As the catalyst mass elevates, the elimination of MO at 60 min rises from 20.89 to 98.76%. Without a catalyst, the removal of MO is significantly limited, indicating low H$_2$O$_2$ activity efficiency. The increase in the dosage of the 5%Fe@BC catalyst from 0.2 to 0.5 g/l leads to a remarkable increase in MO degradation, suggesting a greater number of active sites on the 5%Fe@BC catalyst to activate H$_2$O$_2$ [47]. Increasing the 5%Fe@BC catalyst from 0.5 to 1 g/l slightly improve the degradation of the organic pollutant. It's probable that too

much catalyst has a detrimental impact on how quickly hydroxyl radicals are consumed and lowers the catalytic activity of H$_2$O$_2$.

4.2 Effect of H$_2$O$_2$

In the advanced oxidation process of Fenton-like, hydroxyl radicals are typically present in the solution for the removal of recalcitrant pollutants [48]. The production of OH· is generally linked to the concentration of H$_2$O$_2$. The impact of H$_2$O$_2$ on the degradation of organic matter MO is illustrated in Fig. 7. In the absence of hydrogen peroxide, the rate of discoloration was negligible, reaching only 16.54% within a few minutes, confirming the small role of adsorption. The removal of MO is notably increased with the increase of H$_2$O$_2$ from 0 to 4mM. The hydroxyl radicals required for the breakdown of organic contaminants are thought to increase as H$_2$O$_2$ levels rise [17]. The degradation of MO decrease when the dose increases from 4 to 10mM. This can be attributed to the self-decomposition and negative effect of an excess of H$_2$O$_2$ in the solution. The excess hydrogen peroxide leads to an undesirable scavenging of hydroxyl radicals [49].

4.3 Effect of pH

pH is a key factor in the heterogeneous Fenton-like process, influencing both the catalytic capacity of catalysts for dye degradation [50, 51]. Therefore, it is crucial to find the optimal value. The effect of pH on the degradation of MO is illustrated in Fig. 8. At pH 3, the Fenton like process used achieves a very high discoloration rate of approximated 97% in 60 min. The degradation efficiency of MO reaches
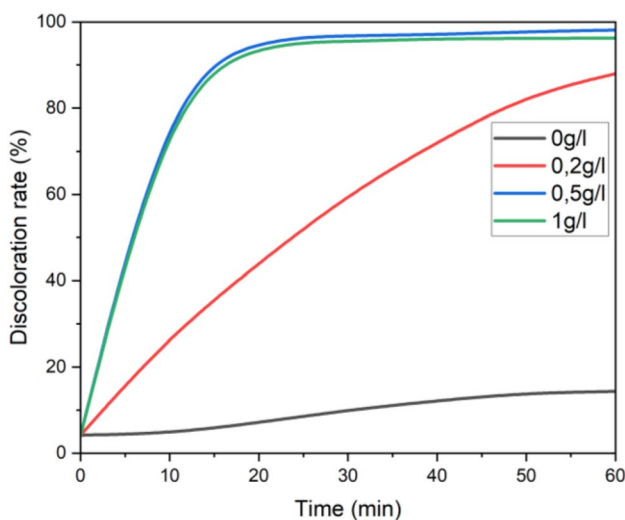
Fig. 6 Effect of catalyst dosage. Experimental conditions: [MO] = 20mg/l, [H$_2$O$_2$] = 2mM, pH 3, T = 30 ± 2 °C
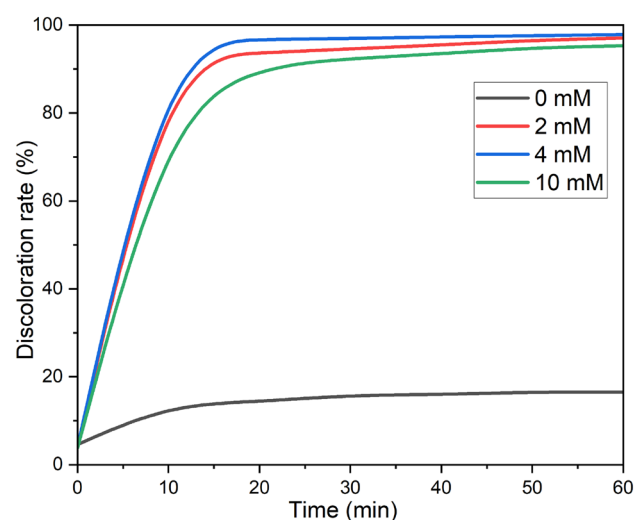
Fig. 7 Effect of H$_2$O$_2$. Experimental conditions: [MO] = 20mg/l, catalyst dose = 0.5g/l, pH 3, T = 30 ± 2 °C
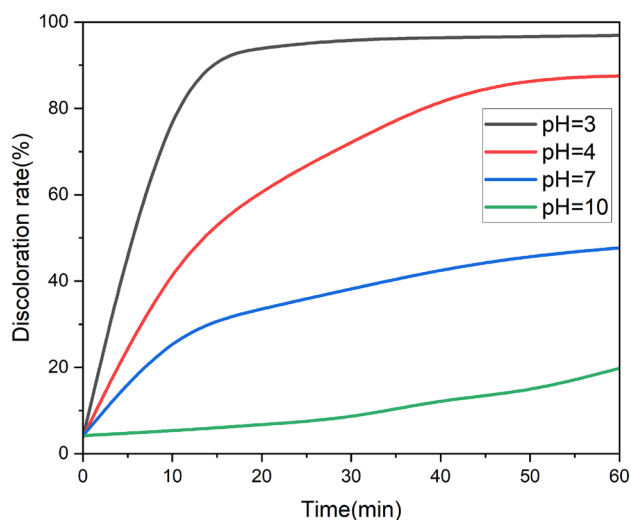
Fig. 8 Effect of pH. Experimental conditions: [MO] = 20 mg/l, [H_2O_2] = 4 mM Catalyst dose = 0.5 g/l, T = 30 ± 2 °C

47.67% at neutral conditions (pH 7). In contrast, the degradation of MO exhibits a significantly low efficiency under basic conditions (pH 10).The decrease can be justified by the precipitation of dissolved iron and the instability of H_2O_2 in the solution [52]. Additionally, the catalyst 5%Fe@BC becomes deactivated, which reduces the production of hydroxyl radicals (OH·). Furthermore, several complexes from in the medium [53]. The pH value of 3 is considered optimal and will be fixer for the subsequent experiments [54].
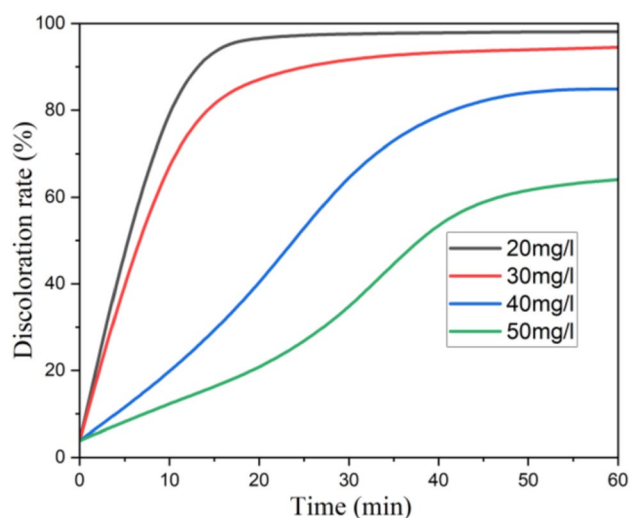
4.4 Effect of MO dose

As illustrated in Fig. 9, the degradation efficiency of organic pollutants gradually declines as the dosage of the pollutant increases. The negative effect of organic pollutants concentration can explain a higher number of organic molecules and reactive intermediates [55]. A higher concentration leads to a weaker catalytic reaction between the Fenton reagents. Furthermore, the intermediate reactions generated on the catalyst surface can inhibit subsequent reactions. A high concentration of organic pollutants requires a high dose of solid catalyst [56]. As the reaction progresses, the catalytic reaction between the catalyst and H_2O_2 may be reduced due to shortage of catalyst.

4.5 Effect of temperature

As shown in Fig. 10, the degradation of the organic pollutant is clearly enhanced with increasing reaction temperature [55]. The decolorization efficiency increases from 62.19% to 98.98% within 60 min when the temperature rises from 15 to 50°C.This is mainly attributed to the increased reaction rate [57], and enhanced collisions between organic pollutants and hydroxyl radicals OH·, which are generated by Fenton-like reaction [58]. On the other hand, a high temperature increas.es the operating cost for a practical application and can be detrimental to catalyst stability, leading to the destruction of the hydrochar support [59].A temperature value of 30 °C is considered optimal and used for the remaining experiments.
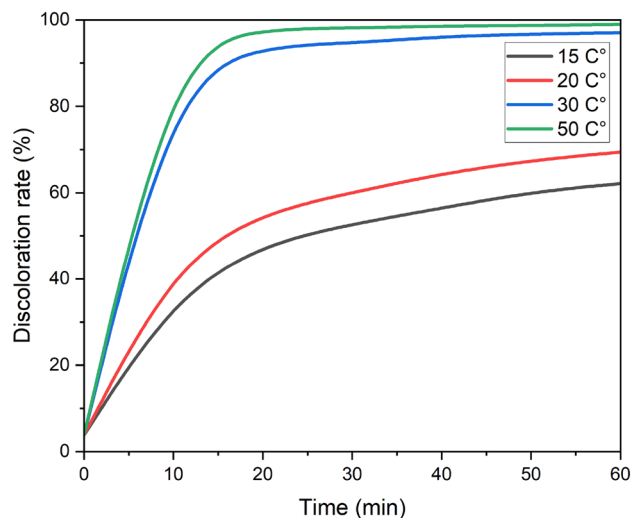

Fig. 9 Effect of MO. Experimental conditions: [H_2O_2] = 4 mM, Catalyst dose = 0.5 g/l, pH 3, T = 30 ± 2 °C

Fig. 10 Effect of temperature. Experimental conditions: [MO] = 20 mg/l, [H_2O_2] = 4mM, catalyst dosage 0.5 g/l, pH 3
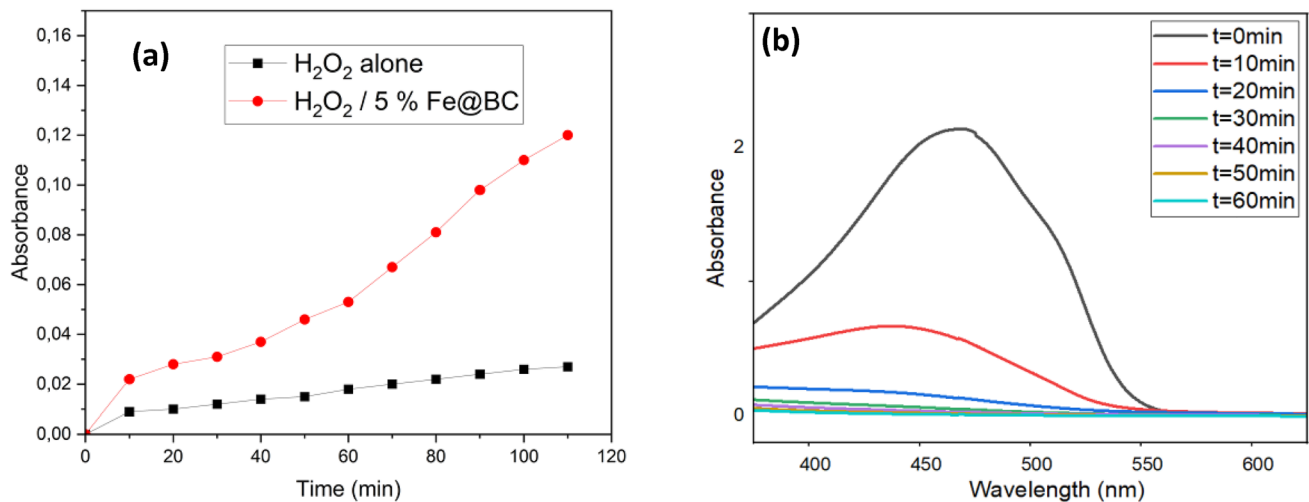
Fig. 11 **a** Salicylic acid absorbance at 300 nm during benzoic acid oxidation; **b** The UV–visible absorption spectra of the MO solution as a function of time

4.6 Generation of hydroxyl radicals (OH·)

To Test the existence of OH· in the heterogeneous Fenton like process, a solution was prepared by adding 100 ml of benzoic acid (BA) to the system. The solution was maintained at pH 3, with a catalyst mass of 0.5 g/L, a 4 mM dose of H_2O_2, and solution temperature of 30 °C [60].There was a gradual increase in absorbance over time during the oxidation process for both Fenton catalysts (H_2O_2 and H_2O_2/5%Fe@BC), as shown in Fig. 11a. This indicates that benzoic acid trapped the OH· radicals and formed salicylic acid [61].In the absence of a catalyst, salicylic acid production was not identified due to insufficient radical production (HO·). The results indicated a continuous generation of hydroxyl radicals that effectively attack the pollutant [62].Fig. 11b shows how the solution's UV–visible spectra changed as it underwent oxidation. Gradually, the band with a wavelength of 464 nm that is ascribed to the conjugated structure created by the azo linkage narrows. This drop demonstrates the deterioration and discoloration of methyl orange caused by the Fenton-like process' cleavage of the chromophore in the dye structure [63].

4.7 Statistical modulization and ideal conditions for pollution removal

The utilization of the Box-Behnken design model aimed to assess the significance of various parameters and identify the ideal experimental conditions for achieving effective oxidation through the heterogeneous Fenton-like process. The removal and discoloration rate of pollutants (Eq. 3), which is the response obtained from planned

Table 3 Box-Behnken design for the three independent variables with discoloration rate

Run	A: [MO] (mg/L)	B: catalyst mass (g)	C: Temperature (°C)	Discoloration rate Actual (%)	Discoloration rate Predicted
1	70	0.55	55	0.940	0.951
2	20	0.55	55	0.970	0.973
3	45	1	55	0.975	0.973
4	45	1	25	0.813	0.827
5	45	0.55	40	0.984	0.980
6	45	0.1	55	0.850	0.835
7	20	0.1	40	0.812	0.823
8	45	0.55	40	0.984	0.980
9	20	1	40	0.974	0.971
10	45	0.55	40	0.970	0.980
11	20	0.55	25	0.880	0.868
12	70	1	40	0.910	0.899
13	70	0.1	40	0.710	0.712
14	45	0.55	40	0.983	0.980
15	70	0.55	25	0.710	0.706
16	45	0.1	25	0.630	0.630

experiments with three variables, pollutant dosage MO, 5%Fe@BC catalyst mass, and the optimal temperature for pollutant degradation through the Fenton-like reaction (Table 1) was studied using an experimental plan comprising four central repetitions. The matrix for estimating the number of tests needed to get the response, especially the discoloration rate, is shown in Table 3. Three variables are represented by the K number of optimal factors. In this context, 16 experiments were completed [64]. The results

Table 4 The degradation of MO using an analysis of variance (ANOVA)

Source	Sum of Squares	df	Mean Square	F-value	p-value	
Model	0.1999	9	0.0222	117.99	< 0.0001	Significant
A: [MO]	0.0167	1	0.0167	88.91	< 0.0001	
B: catalyst mass	0.0560	1	0.0560	297.48	< 0.0001	
C: Temperature	0.0615	1	0.0615	326.77	< 0.0001	
AB	0.0004	1	0.0004	1.93	0.2136	
AC	0.0049	1	0.0049	26.03	0.0022	
BC	0.0009	1	0.0009	4.54	0.0771	
A^2	0.0050	1	0.0050	26.57	0.0021	
B^2	0.0350	1	0.0350	185.68	< 0.0001	
C^2	0.0196	1	0.0196	104.00	< 0.0001	
Residual	0.0011	6	0.0002			
Lack of Fit	0.0010	3	0.0003	6.92	0.0732	Not significant
Pure Error	0.0001	3	0.0000			
Cor Total	0.2010	15				

Std. Dev	0.0137		R^2	0.9944
Mean	0.8809		Adjusted R^2	0.9860
C.V. %	1.56		Predicted R^2	0.9202
Adeq Precision	32.2132			
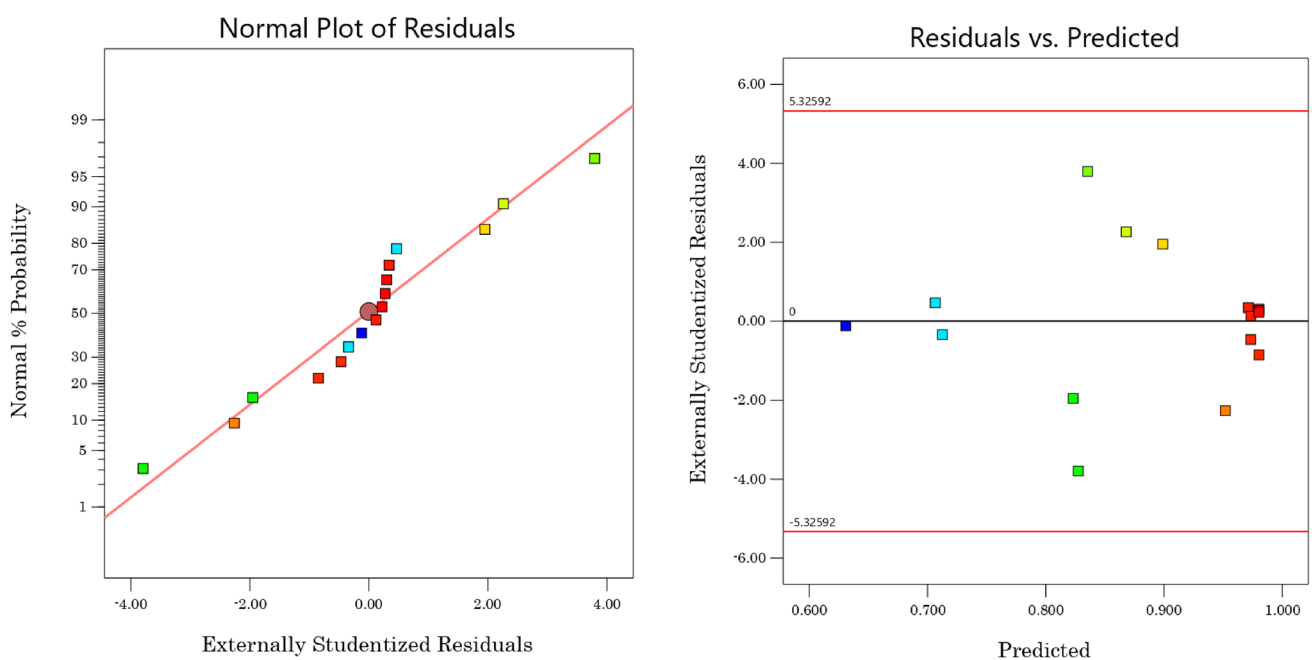
Fig. 12 Predicted values versus actual values of the model for the discoloration rate

are consistent with the combined impact of the three variables within their acceptable range.

ANOVA analysis was performed to assess the validity of the statistical model trials (Table 4). In the ANOVA, the majority of parameters tested to evaluate model validation are the mean square ratio values, significant F-values, and P-values of the confidence interval for model terms, calculated at 95% confidence level. A P-value lower than 5% ensures the significance of the model [65]. As a result, higher F-values (117.99) and low P-values (< 0.0001) for the degradation of refractory organic pollutants confirm the statistical significance and importance of model validation.
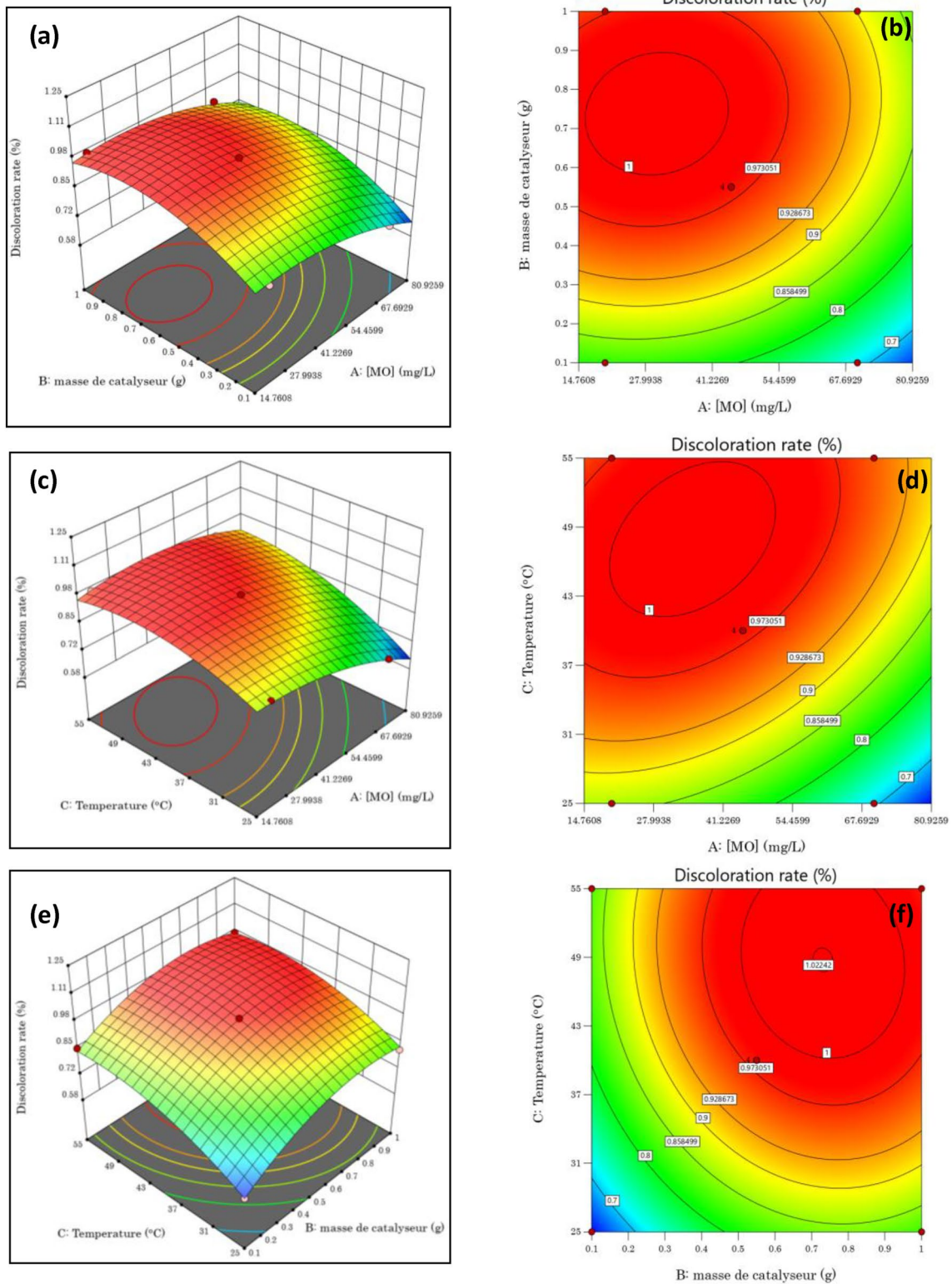
Fig. 13 Response surface traces: Effect of the three variables studied (A, B, C) on discoloration rate

Moreover, the correlation coefficient values (R^2) exhibited a high level of accuracy ($R^2 = 0.99$ with $R^2_{adjusted} = 0.98$, as shown in Table 4). This indicates that the model created is a good fit for the experimental data and possesses strong predictive capabilities [50, 66].Furthermore, the results shown in Fig. 12 reveal a strong correlation between the predicted and experimental values, indicating that the model is appropriate and performs well for the response of organic pollutant degradation. As a result, the second-order polynomial relationship, which was also used to determine the correlation of the three different variables with the Y_i response, was expressed by equation (Eq. 5):

$$Discoloration\ rate\ (\%) = 0.116 - 0.001A + 0.742B + 0.028C + 0.001AB$$
$$+ 9.3\,E^{-05}AC - 0.002BC - 5.6\,E^{-05}A^2 - 0.461B^2 - 0.0003C^2 \tag{5}$$

Figure 13 presents three-dimensional (3D) response surface plots for the discoloration rate as a function of catalyst mass, temperature, and organic pollutant dose (MO). The surface response of discoloration efficiency in the oxidation process, while keeping temperature (°C) and catalyst mass (g/l) as independent variables, is shown in Fig. 13a, b. It was determined that the discoloration rate increases with increasing temperature (from 25 to 55 °C) and catalyst mass (0.1–1 g/l), confirming the interaction between these two parameters [67]. Figure 13c, d show that the effect of catalyst mass is greater than the effect of pollutant dose (14.67–80.92 mg/l) on the discoloration rate. Figure 13e, f demonstrate how the discoloration rate increases with temperature as a function of pollutant dose, with temperature having a more significant impact than the pollutant dose.

The desirability function was employed for numerical optimization purposes. One of the objectives of this study is to maximize the Discoloration rate by utilizing the variables outlined in Table 1S. The desirability function is employed to determine the highest value of function D among various alternatives. The alternative with the highest desirability value, as indicated in Table 4, is selected as the optimal option.

To optimize the process parameters, the Design Expert software was employed, making use of the prediction point feature. The optimized parameters were subsequently determined using the statistical software, and the results were documented in Table 5. To validate the Response Surface Methodology model based on the Box-Behnken Design, experiments were conducted on wastewater solutions using the selected optimization conditions for decolorization. The results showed that the experimental percentage (92.45%) and the predicted decolorization percentage (92%) differed only by 0.45%. Therefore, Eq. 5 was confirmed to accurately calculate the decolorization rate of the solution.

Table 6 compares the results of the 5% Fe@BC catalyst's performance in effectively removing organic matter (MO) with those of another earlier research. This comparison considers numerous methods of treatment, including heterogeneous Fenton, Fenton-like oxidation, employing various solid catalysts, and application under various conditions (pH, amount of H_2O_2, catalyst concentration, reaction time). This comparison shows that, in our study, we acquired significant responses compared to the other catalysts stated, although using a little amount of H_2O_2 and catalyst and a shorter reaction time [68], suggesting that the catalyst is a good candidate for a Fenton-like reaction. These results demonstrate that each catalytic system behaves differently and that the optimum conditions for

Table 5 Verification tests under optimal conditions

Optimal condition: $X_1 = 0.50$ g/l, $X_2 = 35.5$ °C, $X_3 = 50$ mg/L avec D = 1

	Predicted	Experimental	Error (%)
Discoloration rate (%)	92	92,45	0,49

Table 6 Comparison of MO discoloration for various methods and catalysts

Method/catalyst	C (dye) (mg/l)	Concentration H_2O_2 (mmol/l)	Catalyst Concentration (g/l)	pH	Reaction time (min)	Discoloration efficiency (%)	Ref
Fenton-type/Co-SMA	30	37.9	29.92	4.31	30	94.79	[69]
Fenton-like/MIL-100(Fe)/GO	50	8	0.5	3	240	98	[70]
Fenton/Fe-sand	150	5,8	1,5	2.5	60	100	[71]
Fenton-like/5%Fe@BC	50	4	0.5	3	60	93	This work
Fenton-like/Fe2MnO4	50	18	2.5	4	120	100	[72]

achieving maximum MO removal cannot be easily extrapolated from one system to another.

5 Conclusion

The main objective of this research was to explore the possibility of degrading organic pollutants MO by a heterogeneous Fenton-like process, using an environmentally friendly and cost-effective material that is available easily and locally. For the preparation of the heterogeneous catalyst, wood sawdust waste was utilized with a 5% weight doping of iron. Ferrous ions were loaded onto this support (hydrochar), using the hydrothermal carbonization method with the assistance of an autoclave. The degradation of methyl orange depends on the process variables. The decolorization rate reached 92.54% under optimal conditions, which included a catalyst dosage of 0.5 mg/L, an organic pollutant concentration of 50 mg/L, and a temperature of 35.5 °C. The results indicate that the heterogeneous Fenton process based on 5%Fe@BC can be used as a viable alternative to conventional treatment methods for wastewater. In addition, optimization of the Fenton -like process by experimental design such as response surface methodology are also effective tools for reducing the number of experiments and consumables costs. Moreover, since it determines the interaction between variables, it helps us to understand better the effect of independent variables on dependent ones. The advantage of the heterogeneous Fenton process used in this work is to separate easily the solid catalyst (5% Fe@BC) and avoid sludge formation at the end of the treatment. Future studies should focus on the practical application of these materials for the degradation of real pollutants and the optimization of Fenton catalyst production processes.

Declarations

References

1. Asghar A, Raman AAA, Daud WMAW (2015) Advanced oxidation processes for in-situ production of hydrogen peroxide/hydroxyl radical for textile wastewater treatment: a review. J Clean Prod 87(1):826–838. https://doi.org/10.1016/j.jclepro.2014.09.010

2. Askari R et al (2023) Synthesis of activated carbon from cherry tree waste and its application in removing cationic red 14 dye from aqueous environments. Appl Water Sci 13(4):1–12. https://doi.org/10.1007/s13201-023-01899-1

3. Mittal A, Malviya A, Kaur D, Mittal J, Kurup L (2007) Studies on the adsorption kinetics and isotherms for the removal and recovery of Methyl Orange from wastewaters using waste materials. J Hazard Mater 148(1–2):229–240. https://doi.org/10.1016/j.jhazmat.2007.02.028

4. Rahmani A, Azami Gilani R, Dargahi A, Faradmal J (2023) Electro-Fenton/peracetic acid process for the removal of Rhodamine B dye from aqueous media: effect of operational parameters and optimization with Taguchi method. Desalin Water Treat 297:254–263. https://doi.org/10.5004/dwt.2023.29635

5. Taylor P, Gökku Ö, Ço F, Kocao M (2013) Desalination and Water Treatment Determination of optimum conditions for color and COD removal of reactive blue 19 by Fenton oxidation process. Desalination Water Treat. https://doi.org/10.1080/19443994.2013.812523

6. Gürtekin E (2018) Experimental and numerical design of renewable - energy - supported advanced biological wastewater treatment plant. Int J Environ Sci Technol 3:0123456789. https://doi.org/10.1007/s13762-018-2088-x

7. Mohammadifard A, Allouss D, Vosoughi M, Dargahi A, Moharrami A (2022) Synthesis of magnetic Fe_3O_4 / activated carbon prepared from banana peel (BPAC @ Fe_3O_4) and salvia seed (SSAC @ Fe_3O_4) and applications in the adsorption of basic blue 41 textile dye from aqueous solutions. Appl Water Sci 12(5):1–11. https://doi.org/10.1007/s13201-022-01622-6

8. Peyghami A, Moharrami A, Rashtbari Y, Afshin S, Dargahi A (2021) Evaluation of the efficiency of magnetized clinoptilolite zeolite with Fe_3O_4 nanoparticles on the removal of basic violet 16 (BV16) dye from aqueous solutions. J Dispers Sci Technol. https://doi.org/10.1080/01932691.2021.1947847

9. Adachi A et al (2023) Cactus and holm Oak acorn for efficient textile wastewater treatment by coagulation-flocculation

process optimization using box-Benhken design. J Ecol Eng 24(6):315–328. https://doi.org/10.12911/22998993/162784

10. El Ouadrhiri F et al (2023) Nitrogen and phosphorus co-doped carbocatalyst for efficient organic pollutant removal through persulfate-based advanced oxidation processes. J Saudi Chem Soc 27(3):101648. https://doi.org/10.1016/j.jscs.2023.101648

11. Khataee A, Salahpour F, Fathinia M (2015) Journal of Industrial and engineering chemistry Iron rich laterite soil with mesoporous structure for heterogeneous Fenton-like degradation of an azo dye under visible light. J Ind Eng Chem 26:129–135. https://doi.org/10.1016/j.jiec.2014.11.024

12. Wang JL, Xu LJ (2012) Advanced oxidation processes for wastewater treatment: formation of hydroxyl radical and application. Crit Rev Environ Sci Technol 42(3):251–325. https://doi.org/10.1080/10643389.2010.507698

13. Zhang YY, Deng JH, He C, Huang SS, Tian SH, Xiong Y (2010) Application of $Fe_2V_4O_{13}$ as a new multi-metal heterogeneous Fenton-like catalyst for the degradation of organic pollutants. Environ Technol 31(2):145–154. https://doi.org/10.1080/09593330903397755

14. Yang Y, Xu L, Li W, Fan W, Song S, Yang J (2019) Adsorption and degradation of sulfadiazine over nanoscale zero-valent iron encapsulated in three-dimensional graphene network through oxygen-driven heterogeneous Fenton-like reactions. Appl Catal B Environ 259:118057. https://doi.org/10.1016/j.apcatb.2019.118057

15. Radoń A et al (2019) Catalytic activity of non-spherical shaped magnetite nanoparticles in degradation of Sudan I, rhodamine B and methylene blue dyes. Appl Surf Sci 487:1018–1025. https://doi.org/10.1016/j.apsusc.2019.05.091

16. Agú UA, Mendieta SN, Gerbaldo MV, Crivello ME, Casuscelli SG (2020) Highly active heterogeneous fenton-like system based on cobalt ferrite. Ind Eng Chem Res 59(4):1702–1711. https://doi.org/10.1021/acs.iecr.9b04042

17. Xin S et al (2020) High efficiency heterogeneous Fenton-like catalyst biochar modified $CuFeO_2$ for the degradation of tetracycline: economical synthesis, catalytic performance and mechanism. Appl Catal B Environ 280:2021. https://doi.org/10.1016/j.apcatb.2020.119386

18. Li X, Zhou M, Pan Y (2018) Enhanced degradation of 2, 4-dichlorophenoxyacetic acid by pre- magnetization Fe-C activated persulfate : in fl uential factors, mechanism and degradation pathway. J Hazard Mater 353:454–465. https://doi.org/10.1016/j.jhazmat.2018.04.035

19. Li K et al (2019) (2018) Removal of Cr(VI) from water by a biochar-coupled g-C3N4 nanosheets composite and performance of a recycled photocatalyst in single and combined pollution systems. Appl Catal B Environ 243:386–396. https://doi.org/10.1016/j.apcatb.2018.10.052

20. Kayalvizhi K et al (2022) (2021) Adsorption of copper and nickel by using sawdust chitosan nanocomposite beads – A kinetic and thermodynamic study. Environ Res 203:111814. https://doi.org/10.1016/j.envres.2021.111814

21. Douara N, Bestani B, Benderdouche N, Duclaux L (2016) Sawdust-based activated carbon ability in the removal of phenol-based organics from aqueous media. Desalin Water Treat 57(12):5529–5545. https://doi.org/10.1080/19443994.2015.1005151

22. Qiu M et al (2022) Biochar for the removal of contaminants from soil and water: a review. Biochar 4(1):1–25. https://doi.org/10.1007/s42773-022-00146-1

23. Abdel-fattah TM, Mahmoud ME, Ahmed SB, Huff MD, Lee JW, Kumar S (2015) Journal of industrial and engineering chemistry biochar from woody biomass for removing metal contaminants and carbon sequestration. J Ind Eng Chem 22:103–109. https://doi.org/10.1016/j.jiec.2014.06.030

24. El Ouadrhiri F et al (2023) Acid assisted-hydrothermal carbonization of solid waste from essential oils industry: optimization using I-optimal experimental design and removal dye application. Arab J Chem 16(8):104872. https://doi.org/10.1016/j.arabjc.2023.104872

25. Susanti RF, Arie AA, Kristianto H, Erico M, Kevin G, Devianto H (2019) Activated carbon from citric acid catalyzed hydrothermal carbonization and chemical activation of salacca peel as potential electrode for lithium ion capacitor's cathode. Ionics (Kiel) 25(8):3915–3925. https://doi.org/10.1007/s11581-019-02904-x

26. Li Y et al (2018) Hydrochars from bamboo sawdust through acid assisted and two-stage hydrothermal carbonization for removal of two organics from aqueous solution. Bioresour Technol 261:257–264. https://doi.org/10.1016/j.biortech.2018.03.108

27. Fuertes AB et al (2010) Chemical and structural properties of carbonaceous products obtained by pyrolysis and hydrothermal carbonisation of corn stover. Aust J Soil Res 48(6–7):618–626. https://doi.org/10.1071/SR10010

28. Sun A, Zhao H, Wang M, Ma J, Jin H, Zhang K (2022) One-pot synthesis of pyrite nanoplates supported on chitosan hydrochar as Fenton catalysts for organics removal from water. Catalysts. https://doi.org/10.3390/catal12080858

29. Zhang N, Chen J, Fang Z, Tsang EP (2019) Ceria accelerated nanoscale zerovalent iron assisted heterogenous Fenton oxidation of tetracycline. Chem Eng J 369(March):588–599. https://doi.org/10.1016/j.cej.2019.03.112

30. Chen ZX, Jin XY, Chen Z, Megharaj M, Naidu R (2011) Removal of methyl orange from aqueous solution using bentonite-supported nanoscale zero-valent iron. J Colloid Interface Sci 363(2):601–607. https://doi.org/10.1016/j.jcis.2011.07.057

31. Pourali P, Fazlzadeh M, Aaligadri M, Dargahi A, Poureshgh Y, Kakavandi B (2022) Enhanced three-dimensional electrochemical process using magnetic recoverable of $Fe_3O_4@GAC$ towards furfural degradation and mineralization. Arab J Chem 15(8):103980. https://doi.org/10.1016/j.arabjc.2022.103980

32. Hasani K, Peyghami A, Moharrami A, Vosoughi M, Dargahi A (2020) The efficacy of sono-electro-Fenton process for removal of Cefixime antibiotic from aqueous solutions by response surface methodology (RSM) and evaluation of toxicity of effluent by microorganisms. Arab J Chem 13(7):6122–6139. https://doi.org/10.1016/j.arabjc.2020.05.012

33. El Ouadrhiri F, Elyemni M, Lahkimi A, Lhassani A, Chaouch M, Taleb M (2021) Mesoporous carbon from optimized date stone hydrochar by catalytic hydrothermal carbonization using response surface methodology: application to dyes adsorption. Int J Chem Eng 2021:5555406. https://doi.org/10.1155/2021/5555406

34. Xu L, Wu C, Liu P, Bai X, Du X, Jin P (2020) Peroxymonosulfate activation by nitrogen-doped biochar from sawdust for the efficient degradation of organic pollutants. Chem Eng J. https://doi.org/10.1016/j.cej.2020.124065

35. Wang P et al (2017) Synthesis and application of iron and zinc doped biochar for removal of p-nitrophenol in wastewater and assessment of the influence of co-existed Pb(II). Appl Surf Sci 392:391–401. https://doi.org/10.1016/j.apsusc.2016.09.052

36. Kumar P, Kumar P, Rao PVC, Choudary NV, Sriganesh G (2017) Saw dust pyrolysis: effect of temperature and catalysts. Fuel 199:339–345. https://doi.org/10.1016/j.fuel.2017.02.099

37. Sikdar D, Goswami S, Das P (2021) Synthesis of activated carbon material using sawdust as precursor and its application for dye removal: batch study and optimization using response surface methodology. Biomass Convers Biorefinery. https://doi.org/10.1007/s13399-021-01385-1

38. Tang L et al (2016) Removal of bisphenol A by iron nanoparticle-doped magnetic ordered mesoporous carbon. RSC Adv 6(31):25724–25732. https://doi.org/10.1039/c5ra27710h

39. Zhang P, Tan X, Liu S, Liu Y, Zeng G, Ye S (2019) Catalytic degradation of estrogen by persulfate activated with iron-doped graphitic biochar: process variables effects and matrix effects. Chem Eng J 378:122141. https://doi.org/10.1016/j.cej.2019.122141

40. Li H, Shi B, Fu X, Zhang H, Yang H (2023) Journal of environmental chemical engineering preparation and application of red mud-based zero-valent iron heterogeneous Fenton catalyst : a new idea for red mud recycling. J Environ Chem Eng 11(3):109998. https://doi.org/10.1016/j.jece.2023.109998

41. Greaves C (1983) A powder neutron diffraction investigation of vacancy ordering and covalence in 7-Fe_2Oa. J Solid State Chem 333:325–333

42. Xu X, Chen W, Zong S, Ren X, Liu D (2019) Atrazine degradation using Fe_3O_4 -sepiolite catalyzed persulfate : reactivity, mechanism and stability. J Hazard Mater 377(May):62–69. https://doi.org/10.1016/j.jhazmat.2019.05.029

43. Gai C, Zhang F, Lang Q, Liu T, Peng N, Liu Z (2017) Facile one-pot synthesis of iron nanoparticles immobilized into the porous hydrochar for catalytic decomposition of phenol. Appl Catal B Environ 204:566–576. https://doi.org/10.1016/j.apcatb.2016.12.005

44. Jung KW, Lee SY, Lee YJ, Choi JW (2019) Ultrasound-assisted heterogeneous Fenton-like process for bisphenol a removal at neutral pH using hierarchically structured manganese dioxide/biochar nanocomposites as catalysts. Ultrason Sonochem 57:22–28. https://doi.org/10.1016/j.ultsonch.2019.04.039

45. Chu JH, Kang JK, Park SJ, Lee CG (2020) Application of magnetic biochar derived from food waste in heterogeneous sono-Fenton-like process for removal of organic dyes from aqueous solution. J Water Process Eng 37:101455. https://doi.org/10.1016/j.jwpe.2020.101455

46. Xie Y et al (2020) FexP/biochar composites induced oxygen-driven Fenton-like reaction for sulfamethoxazole removal: performance and reaction mechanism. Chem Eng J 396:125321. https://doi.org/10.1016/j.cej.2020.125321

47. Rubeena KK, Hari Prasad Reddy P, Laiju AR, Nidheesh PV (2018) Iron impregnated biochars as heterogeneous Fenton catalyst for the degradation of acid red 1 dye. J Environ Manage 226:320–328. https://doi.org/10.1016/j.jenvman.2018.08.055

48. Wang C, Cao Y, Wang H (2019) Copper-based catalyst from waste printed circuit boards for effective Fenton-like discoloration of Rhodamine B at neutral pH. Chemosphere 230:278–285. https://doi.org/10.1016/j.chemosphere.2019.05.068

49. Deng J et al (2018) Nanoscale zero-valent iron/biochar composite as an activator for Fenton-like removal of sulfamethazine. Sep Purif Technol 202(March):130–137. https://doi.org/10.1016/j.seppur.2018.03.048

50. Adachi A et al (2022) Decolorization and degradation of methyl orange azo dye in aqueous solution by the electro fenton process: application of optimization. Catalysts 12(6):665. https://doi.org/10.3390/catal12060665

51. Fu F, Wang Q, Tang B (2010) Effective degradation of C.I. Acid Red 73 by advanced Fenton process. J Hazard Mater 174(1–3):17–22. https://doi.org/10.1016/j.jhazmat.2009.09.009

52. Yao Y et al (2013) Efficient removal of dyes using heterogeneous Fenton catalysts based on activated carbon Fibers with enhanced activity. Chem Eng Sci 101:424–431. https://doi.org/10.1016/j.ces.2013.06.009

53. Daud NK, Ahmad MA, Hameed BH (2010) Decolorization of Acid Red 1 dye solution by Fenton-like process using Fe-Montmorillonite K10 catalyst. Chem Eng J 165(1):111–116. https://doi.org/10.1016/j.cej.2010.08.072

54. Heidari M, Vosoughi M, Sadeghi H, Dargahi A, Mokhtari SA (2021) Degradation of diazinon from aqueous solutions by electro-Fenton process: effect of operating parameters, intermediate identification, degradation pathway, and optimization using response surface methodology (RSM). Sep Sci Technol 56(13):2287–2299. https://doi.org/10.1080/01496395.2020.1821060

55. Yuan W, Zhang C, Wei H, Wang Q, Li K (2017) In situ synthesis and immobilization of a Cu(II)-pyridyl complex on silica microspheres as a novel Fenton-like catalyst for RhB degradation at near-neutral pH. RSC Adv 7(37):22825–22835. https://doi.org/10.1039/c7ra02916k

56. Park J, Wang JJ, Xiao R, Tafti N, Delaune RD, Seo D (2017) Bioresource technology degradation of orange G by Fenton-like reaction with Fe-impregnated biochar catalyst". Bioresour Technol 249:368–376. https://doi.org/10.1016/j.biortech.2017.10.030

57. Idel-aoud R, Valiente M, Yaacoubi A, Tanouti B, López-Mesas M (2011) Rapid decolourization and mineralization of the azo dye C.I. Acid Red 14 by heterogeneous Fenton reaction. J Hazard Mater 186(1):745–750. https://doi.org/10.1016/j.jhazmat.2010.11.056

58. Yu Y et al (2019) Heterogeneous fenton-like degradation of ofloxacin over sludge derived carbon as catalysts: mechanism and performance. Sci Total Environ 654:942–947. https://doi.org/10.1016/j.scitotenv.2018.11.156

59. Titouhi H, Belgaied JE (2016) Heterogeneous Fenton oxidation of ofloxacin drug by iron alginate support. Environ Technol 37(16):2003–2015. https://doi.org/10.1080/09593330.2016.1139630

60. Satoh AY, Trosko JE, Masten SJ (2007) Methylene blue dye test for rapid qualitative detection of hydroxyl radicals formed in a Fenton's reaction aqueous solution. Environ Sci Technol 41(8):2881–2887. https://doi.org/10.1021/es0617800

61. Gazi S, Ananthakrishnan R (2011) Semi-quantitative determination of hydroxyl radicals by benzoic acid hydroxylation: an analytical methodology for photo-Fenton systems. Curr Anal Chem 8(1):143–149. https://doi.org/10.2174/157341112798472297

62. Laiju AR, Sivasankar T, Nidheesh PV (2014) Iron-loaded mangosteen as a heterogeneous Fenton catalyst for the treatment of landfill leachate. Environ Sci Pollut Res 21(18):10900–10907. https://doi.org/10.1007/s11356-014-2883-y

63. Chen YP, Liu SY, Yu HQ, Yin H, Li QR (2008) Radiation-induced degradation of methyl orange in aqueous solutions. Chemosphere 72(4):532–536. https://doi.org/10.1016/j.chemosphere.2008.03.054

64. Eid M, Ali M, Abdelsalam H, Ammar NS, Ibrahim HS (2018) Response surface methodology for optimization of the adsorption capability of ball-milled pomegranate peel for different pollutants. J Mol Liq 250:433–445. https://doi.org/10.1016/j.molliq.2017.12.025

65. Naveen NR, Kurakula M, Gowthami B (2020) Materials today : proceedings process optimization by response surface methodology for preparation and evaluation of methotrexate loaded chitosan nanoparticles. Mater Today Proc 33:2716–2724. https://doi.org/10.1016/j.matpr.2020.01.491

66. Alizadeh S, Sadeghi H, Vosoughi M, Dargahi A, Mokhtari SA (2022) Removal of humic acid from aqueous media using Sono-Persulphate process: optimization and modelling with response surface methodology (RSM). Int J Environ Anal Chem 102(16):3707–3721. https://doi.org/10.1080/03067319.2020.1772777

67. Umamaheswari J, Bharathkumar T, Shanthakumar S, Gothandam KM (2020) A feasibility study on optimization of combined advanced oxidation processes for municipal solid waste leachate treatment. Process Saf Environ Prot 143:212–221. https://doi.org/10.1016/j.psep.2020.06.040

68. Xu HY et al (2016) Heterogeneous Fenton-like discoloration of methyl orange using Fe3O4/MWCNTs as catalyst: process

optimization by response surface methodology. Front Mater Sci 10(1):45–55. https://doi.org/10.1007/s11706-016-0326-z

69. Mahamallik P, Pal A (2020) Photo-Fenton process in Co (II)-adsorbed admicellar soft-template on alumina support for methyl orange degradation. Catal Today 348:212–222. https://doi.org/10.1016/j.cattod.2019.07.045

70. Tang J, Wang J (2017) Fe-based metal organic framework/graphene oxide composite as an efficient catalyst for Fenton-like degradation of methyl orange. RSC Adv 7(80):50829–50837. https://doi.org/10.1039/c7ra10145g

71. Omri A, Hamza W, Benzina M (2020) Photo-Fenton oxidation and mineralization of methyl orange using Fe-sand as effective heterogeneous catalyst. J Photochem Photobiol A Chem 393:112444. https://doi.org/10.1016/j.jphotochem.2020.112444

72. Dung T, Hoa N, Huy M, Tham K (2011) Magnetic Fe_2MO_4 (M : Fe, Mn) activated carbons: fabrication, characterization and heterogeneous Fenton oxidation of methyl orange. J Hazard Mater 185(2–3):653–661. https://doi.org/10.1016/j.jhazmat.2010.09.068